Biophysical Journal, Volume *116*

Supplemental Information

Continuum Gating Current Models Computed with Consistent Interactions

Tzyy-Leng Horng, Robert S. Eisenberg, Chun Liu, and Francisco Bezanilla

1. Non-dimensionalization

We non-dimensionalize all physical quantities as follows,

$\tilde{c}_i = \frac{c_i}{c_0},\ \tilde{\phi} = \frac{\phi}{k_B T/e}, \tilde{U} = \frac{U}{k_B T},\ \tilde{s} = \frac{s}{R},\ \tilde{t} = \frac{t}{R^2/D_x},\ \widetilde{D}_i = \frac{D_i}{D_x},\ \tilde{g}_{ij} = \frac{g_{ij}}{k_B T/c_0},\ \tilde{J}_i = \frac{J_i}{c_0 D_x/R},$

$\tilde{I} = \frac{I}{e c_0 D_x R},$

where c_i is concentration of species *i*, with *i*=Na^+, Cl^-, 1, 2, 3, and 4. Each is scaled by c_0 which is the bulk concentration of NaCl in the intracellular/extracellular domains. Here c_0 is set to be 184 mM, equal on both sides, so that the Debye length $\lambda_D = \sqrt{\frac{\varepsilon_r \varepsilon_0 k_B T}{c_0 e^2}}$ is 1nm when the relative permittivity $\varepsilon_r = 80$. ϕ is the electric potential scaled by $k_B T/e$ with k_B being the Boltzmann constant; T the temperature; *e* the elementary charge. All relevant external potentials *U* are scaled by $k_B T$. All sizes *s* are scaled by *R*, which is the radius of vestibule as shown in Fig. 1(b). *R*=1nm here. The time *t* is scaled by R^2/D_x, with D_x being a diffusion coefficient that can be adjusted later to be consistent with the time spans of on/off currents measured in experiments (caused by the movement of arginines). The diffusion coefficient of species *i* is scaled by D_x. The coupling constant g_{ij} of PNP-steric model based on combining rules of Lennard Jones, representing the strength of steric interaction between species *i* and *j*, is scaled by $k_B T/c_0$ [1,2]. For simplicity, we assume $g_{ij} = \begin{cases} g, & \text{for all } i \neq j \\ 0, & \text{for all } i = j \end{cases}$, $i, j = 1,2,3,4$. Note that here we only consider steric interaction among arginines. We think they are a crucial source of correlated structural change and motion (of mass and charge). The consideration of steric effect among arginines is justified by the fact that arginines are generally crowded in hydrophobic plug and vestibules. The flux density of species *i*, J_i, is scaled by $c_0 D_x/R$, and therefore the electric current *I* is scaled by $e c_0 D_x R$. For simplicity of notation, we will drop ~ for all dimensionless quantities shown in all equations.

2. Shape of potential of mean force (PMF) in the hydrophobic plug

Here, we simply assume a hump shape for PMF in the hydrophobic plug as,

$$\begin{cases} V_b = V_{b,max}\left(\tanh\left(5(z - L_R)\right) - \tanh\left(5(z - L - L_R)\right) - 1\right), & \text{when } z \text{ is in zone 2,} \\ V_b = 0, & \text{when } z \text{ is in zone 1 and 3,} \end{cases} \quad \text{(S1)}$$

with $V_{b,max}$ set to be 5 for a good agreement with experimental measurements.

Theoretically, if we set $V_{b,max}$ too large, the gating current would be slow and perhaps small because it would be very difficult for arginines to move across this barrier. The double *tanh* functions are designed to smooth the otherwise top-hat-shape barrier profile, which is not good for numerical differentiation because of its awkward infinite slopes. This smoothing is simply based on the belief that the energy barrier in a protein structure does not have a jump. In future work, it would be wise to compute the PMF from a specific model of charge distribution (both permanent and polarization) constructed from a combination of structural data and molecular dynamics simulations, if feasible.

3. Governing equations derivation from energy variation methods

Governing equations Eqs. (1-4) were derived by energy variational methods based on the following energy (in dimensional form):

$$E = \int_V \left[k_B T \sum_{all\ i} c_i log c_i - \frac{\varepsilon_0 \varepsilon_r}{2} |\nabla \phi|^2 + \sum_{all\ i} q_i e\, c_i \phi + \sum_{arginines} (V_i + V_b)\, c_i + \sum_{arginines\ i,j} \frac{g_{ij}}{2} c_i c_j \right] dV, \quad \text{(S.2)}$$

where the first term is entropy; second and third terms are electrostatic energy; the fourth term is the constraint and barrier potential for arginines; the last term is the steric energy term, based on Lennard-Jones potential [1,3]. The Poisson equation Eq. (1) is derived from the variation of energy with respect to electric potential

$$\frac{\delta E}{\delta \phi} = 0,$$

and species flux densities in Eqs. (3,4) are derived by

$$\mu_i = \frac{\delta E}{\delta c_i}, \qquad J_i = -\frac{D_i}{k_B T} c_i \nabla \mu_i,$$

where μ_i is the chemical potential of species *i*.

4. Quasi-steadiness assumption for Na^+ and Cl^-

Here we assume quasi-steady state for Na^+ and Cl^-, which means $\frac{\partial c_i}{\partial t} = 0, i =$ Na, Cl. The steady state assumption here is justified by the fact that the diffusion coefficients of Na^+ and Cl^- in vestibules are much larger than the diffusion coefficient of arginine based on the very narrow time span of the leading spike of gating current measured in experiments. The spike comes from the linear capacitive current of vestibule when the command potential suddenly rises or drops. This quasi-steady state assumption is essential for the success of our

calculations. Otherwise using realistic diffusion coefficients for Na^+ and Cl^- would render Eqs. (1-4) too stiff to integrate in time. The spike contaminating the gating current is removed in experiments by a simple technique called ***P/n*** leak subtraction (see Section 11; n typically is 4). ***P/n*** leak subtraction is also used to subtract the linear capacity current of all the membranes in the real system that are not included in our model. How to do leak subtraction computationally will be discussed in Section 10.

5. Formulation of boundary conditions

Types of boundary conditions are illustrated in Fig. 1(b). Note the no-flux boundary conditions specified in Fig. 1(b). One prevents Na^+ and Cl^- from entering the hydrophobic plug (zone 2) with low dielectric coefficient. The other boundary condition constrains S4 motion and so prevents the arginines from leaving the vestibules into intracellular/extracellular domains.

Boundary and interface conditions for electric potential ϕ are

$$\phi(0) = V, \quad \phi(L_R^-) = \phi(L_R^+), \quad \Gamma(L_R^-)A(L_R^-)\frac{d\phi}{dz}(L_R^-) = \Gamma(L_R^+)A(L_R^+)\frac{d\phi}{dz}(L_R^+),$$

$$\phi(L_R + L^-) = \phi(L_R + L^+), \quad \Gamma(L_R + L^-)A(L_R + L^-)\frac{d\phi}{dz}(L_R + L^-) = \Gamma(L_R +$$

$$L^+)A(L_R + L^+)\frac{d\phi}{dz}(L_R + L^+), \quad \phi(2L_R + L) = 0. \qquad \text{(S.3)}$$

These are Dirichlet boundary conditions at both ends and continuity of electric potential and displacement at the interfaces between zones. Boundary and interface conditions for arginine are

$$J_i(0,t) = J_i(2L_R + L, t) = 0, \quad c_i(L_R^+, t) = c_i(L_R^-, t), \quad A(L_R^-)J_i(L_R^-, t) = A(L_R^+)J_i(L_R^+, t), \quad c_i(L_R + L^-, t) = c_i(L_R + L^+, t), \quad A(L_R + L^-)J_i(L_R + L^-, t) = A(L_R + L^+)J_i(L_R + L^+, t), \quad i = 1,2,3,4, \qquad \text{(S.4)}$$

where no-flux boundary conditions are placed at both ends of the gating pore, consisting of vestibules and hydrophobic plug, to prevent arginines and S4 from entering intracellular/extracellular domains. The others are continuity of concentration and flux at interfaces between zones. Boundary conditions for Na^+ and Cl^- are

$$c_{Na}(0,t) = c_{Cl}(0,t) = c_{Na}(2L_R + L, t) = c_{Cl}(2L_R + L, t) = 1,$$

$$J_{Na}(L_R, t) = J_{Cl}(L_R, t) = J_{Na}(L_R + L, t) = J_{Cl}(L_R + L, t) = 0, \qquad \text{(S.5)}$$

where Dirichlet boundary conditions are placed at both ends of the gating pore to describe the concentrations for Na^+ and Cl^- as the bulk concentration. No-flux boundary conditions at both ends of hydrophobic plug describe the

impermeability of Na^+ and Cl^- into hydrophobic plug.

6. Parameters fitting

We have tried and found D_i=50, i=1,2,3,4, K=3, K_{S4}=3, b_{S4}=1.5 provide the best fit to the important experiments reported in [4]. Several things are to be noted about the parameter values specified above: (1) there is no experimental measurement of diffusion coefficient of arginine inside vestibule and plug available that we can use for simulation. Imprecise setting of the values of these diffusion coefficients only affects the scale of time in I-V curve, but not its shape. That is why we set time coordinate to be in an arbitrary unit later in results, and here we only focus on comparing the shape of IV curves with experiments in [4]. (2) K, K_{S4}, and b_{S4} were particularly determined by fitting with QV curve in experiment [4]. The QV curve is very sensitive to K and K_{S4}, and many efforts have been taken to achieve proper values for them. The method of fitting is done by trial and error. Choosing incorrect K and K_{S4} would end up serious mismatch of QV curve with experiment [4] as demonstrated by the case of K=3 and K_{S4}=12 in Fig. 1 here. The choice of K=3 and K_{S4}=3 fits experiment [4] best and is adopted for the rest of simulations.

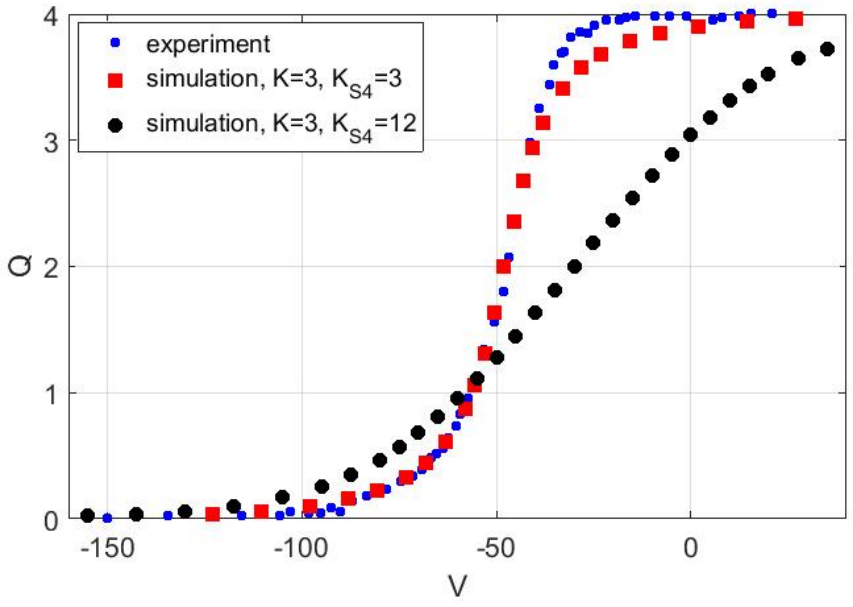

Figure 1. Simulated QV curves under different K and K_{S4} compared with experimental counterpart from [4]. Note that the experimental data in [4] was scaled to 4e.

7. Derivation of Ampere's law in Maxwell's equations by Poisson equation

and species transport equation

Eq. (8) is consistent with Ampere's law in Maxwell's equations:

$$\nabla \times \left(\frac{\vec{B}}{\mu_0}\right) = \varepsilon_0 \varepsilon_r \frac{\partial \vec{E}}{\partial t} + \vec{J}, \qquad \text{(S.6)}$$

or equivalently,

$$\nabla \cdot \left(\varepsilon_0 \varepsilon_r \frac{\partial \vec{E}}{\partial t} + \vec{J}\right) = 0, \qquad \text{(S.7)}$$

where $\vec{E}$ is the electric field and $\vec{J}$ is flux density of charge (current density). Eq. (S.7) tells us that the total current is conserved everywhere and it consists of flux of charges $\vec{J}$ and displacement current $\varepsilon_0 \varepsilon_r \frac{\partial \vec{E}}{\partial t}$. Eq. (S.7) can be derived from the Poisson equation and species transport equation like Eq. (1) and Eq. (2). Starting from Poisson equation in dimensional form:

$$-\nabla \cdot (\varepsilon_0 \varepsilon_r \nabla \phi) = \rho + \sum_i q_i e c_i, \qquad \text{(S.8)}$$

or equivalently

$$\nabla \cdot \left(\varepsilon_0 \varepsilon_r \vec{E}\right) = \rho + \sum_i q_i e c_i. \qquad \text{(S.9)}$$

Taking time derivative of Eq. (S.9),

$$\nabla \cdot \left(\varepsilon_0 \varepsilon_r \frac{\partial \vec{E}}{\partial t}\right) = \sum_i q_i e \frac{\partial c_i}{\partial t}, \qquad \text{(S.10)}$$

and using species transport equation based on mass conservation,

$$\frac{\partial c_i}{\partial t} + \nabla \cdot \vec{J}_i = 0, \qquad \text{(S.11)}$$

then

$$\nabla \cdot \left(\varepsilon_0 \varepsilon_r \frac{\partial \vec{E}}{\partial t}\right) = \sum_i q_i e \frac{\partial c_i}{\partial t} = -\nabla \cdot \sum_i q_i e \vec{J}_i = -\nabla \cdot \vec{J}, \qquad \text{(S.12)}$$

which becomes exactly Eq. (S.7) by defining

$$\vec{J} = \sum_i q_i e \vec{J}_i. \qquad \text{(S.13)}$$

A more general treatment that does not involve assumptions about ε_r can be found in [5-7].

Casting Eq. (S.7) into the present 1D framework by integrating it in space and applying the divergence theorem, we have

$$\varepsilon_0 \varepsilon_r A(z) \frac{\partial E(z,t)}{\partial t} + I(z,t) = \varepsilon_0 \varepsilon_r A(0) \frac{\partial E(0,t)}{\partial t} + I(0,t). \qquad \text{(S.14)}$$

Comparing with Eq. (11),

$$\varepsilon_0 \varepsilon_r A(z) \frac{\partial E(z,t)}{\partial t} - \varepsilon_0 \varepsilon_r A(0) \frac{\partial E(0,t)}{\partial t} = I_{disp}(z,t), \qquad \text{(S.15)}$$

which justifies the naming of displacement current in Eq. (11).

8. Numerical method

High-order multi□block Chebyshev pseudospectral methods are used here to discretize Eqs. (1-4) in space [8]. The resultant semi discrete system is then a set of coupled ordinary differential equations in time and algebraic equations (an ODAE system) [9]. The ordinary differential equations are chiefly from Eq. (2), and algebraic equations are chiefly from Eq. (1) and boundary/interface conditions Eqs. (S.3-S.5). This system is further integrated in time by an ODAE solver (ODE15S in MATLAB (The MathWorks, Natick, MA) [10,11]) together with appropriate initial condition. ODE15S is a variable order variable step (VSVO) solver, which is highly efficient in time integration because it adjusts the time step and order of integration. High□order pseudospectral methods generally provide excellent spatial accuracy with economically practicable resolutions. A combination of these two techniques makes the whole computation very efficient. This is particularly important here, since numerous computations have to be tried during the tuning of parameters. Efficiency will be vital in future calculations comparing theory and experiment in a wide variety of mutants and experimental conditions.

9. Computation of flux of charge, displacement current and total current

According to definition in Eq. (10), flux of charges at the middle of gating pore, $I(L_R + L/2, t)$, and both ends of gating pore, $I(0,t)$ and $I(2L_R + L, t)$, should be computed by

$$I\left(L_R + \frac{L}{2}, t\right) = A\left(L_R + \frac{L}{2}\right)\sum_{arginines} q_i J_i\left(L_R + \frac{L}{2}, t\right), \qquad \text{(S.16)}$$

$$I(0,t) = A(0)\sum_{i=Na,Cl} q_i J_i(0,t), \qquad \text{(S.17)}$$

$$I(2L_R + L, t) = A(2L_R + L)\sum_{i=Na,Cl} q_i J_i(2L_R + L, t). \qquad \text{(S.18)}$$

Except $I\left(L_R + \frac{L}{2}, t\right)$, $I(0,t)$ and $I(2L_R + L, t)$ are trivially zero due to the implement of quasi-steadiness $\frac{\partial c_i}{\partial t} = 0, i = \text{Na, Cl}$, in vestibules, which causes J_{Na} and J_{Cl} to be uniform in vestibules by Eq. (2), and further become zero by the no-flux boundary conditions for Na^+ and Cl^- at the bottom of vestibules as described in Eq. (S.5). We have to alternatively reconstruct $I(0,t)$ and $I(2L_R + L, t)$ by charge conservation of Na^+ and Cl^-,

$$I(0,t) = \frac{d}{dt}\int_0^L A(z)\sum_{Na,Cl} q_i c_i dz, \qquad \text{(S.19)}$$

$$I(2L_R + L, t) = -\frac{d}{dt}\int_{L+L_R}^{L+2L_R} A(z)\sum_{Na,Cl} q_i c_i dz. \qquad \text{(S.20)}$$

After obtaining $I(0,t)$ and $I(2L_R+L,t)$, we can further reconstruct the flux of charges $I(z,t)$ at zone 1 and zone 3 by (8) and (9),

$$I(z,t) = I(0,t) - \frac{d}{dt}\int_0^z A(z)\sum_{all\ i} q_i c_i dz\,,\quad z \in [0, L_R], \qquad \text{(S.21)}$$

$$I(z,t) = I(2L_R+L,t) + \frac{d}{dt}\int_z^{2L_R+L} A(z)\sum_{all\ i} q_i c_i dz\,,\quad z \in [L_R+L, 2L_R+L]. \text{ (S.22)}$$

Flux of charge at zone 2 is simply

$I(z,t) = A(z)\sum_{arginines} q_i J_i(z,t),\ z \in [L_R, L_R+L],$ (S.23)

since Na^+ and Cl^- are not allowed to enter zone 2, the hydrophobic plug.

10. Removing spike in total current

In voltage-clamp experiments, subtracting this linear capacitive component and removing the spike from gating current is done by 'leak subtraction', in various forms, e.g., P/4 (see details in Section 11) In reality, this linear capacitive current that is subtracted in this procedure comes from both the lipid bilayer membrane in parallel with the gating pore. Here, we only considered the capacitive current from solution EDL of vestibule inside the gating pore and ignored the membrane capacitive current because we simply use Dirichlet boundary conditions for ϕ at both ends of the gating pore in Eq. (S.3). Actually, capacitive current of the membrane in parallel with the gating pore would be much larger than vestibule capacitive current. Following the idea of the experiment [4], we calculated $I(0,t)$ with *V* rising from -150 mV to -140 mV at *t*=10, and dropping back to -150 mV at *t*=150. We chose from -150 mV to -140 mV because essentially none of the arginines move across the hydrophobic plug in this hyperpolarized region. The voltage step quickly charges and discharges solution EDL in vestibules, and the computed time course of $I(0,t)$ is just two spikes at on and off of the command potential. Subtracting this hyperpolarized $I(0,t)$, multiplied by a proportion factor (due to the linearity of capacitive current), from its original counterpart will then remove the spikes, and the unspiked $I(0,t)$ is shown in Fig. 5(a). In preliminary calculations with the model, when the command voltage pulse rises faster, the early spike becomes larger and is still visible even after subtraction, suggesting that is the origin of the early transient gating current in experiments [12-14].

11. Removing linear capacitive current to obtain gating current in experiments

Our computations have limited fidelity at short times because of time step limitations in integrating stiff systems. The spike artifacts are one example, described previously. Experimental measurements [12,15] of the fast transient

gating current are fascinating and our calculations will be extended to explore more of them in future study by using greater resolution in time.

A more general consideration is the subtraction procedure used in experiments to isolate gating current from currents arising from other sources. Channels and their voltage sensors are embedded in lipid membranes, therefore they are 'in parallel' with large capacitive currents of the lipid bilayer. The lipid membrane has a large capacitance ($C_{lipid} \cong 8 \times 10^{-7}$ farads/cm^2) that has nothing to do with the current produced by charge movement in the voltage sensor. Fortunately, the capacitance C_{lipid} is a nearly ideal circuit element and the current to charge it is entirely a displacement current accurately described by $i_{cap} = C_{lipid}\, \partial \mathrm{V}/\partial \mathrm{t}$ with a single constant C_{lipid}. V is the voltage across the lipid capacitor. Note that i_{cap} does not include any current or flux of charge carried across the lipid.

In experimental measurements, i_{cap} is always present. Experimental measurements always mix the displacement currents of lipid membrane and voltage sensor. Lipid membrane current usually dominates the measurement of gating currents in native preparations and remains large in systems mutated to have unnaturally large numbers of voltage sensors.

A procedure to remove the lipid membrane current is needed if the gating current of the voltage sensor is to be measured. The procedure introduced by [16] has been used ever since in the improved P/4 version developed by [17] reviewed and discussed in [18]. Also, see another approach in [19] and [20]. Schneider and Chandler's procedure [19] estimates the so-called linear current $i_x = C_x\, \partial \mathrm{V}/\partial \mathrm{t}$ in conditions in which the voltage sensor and C_x behave as ideal circuit elements. The voltage sensor might then have a component linear in potential. An ideal capacitor has a capacitance C_x independent of voltage, time, current, or ionic composition. The Schneider procedure then subtracts that linear current i_x—plus any linear component of voltage sensor current—from the total current measured in conditions in which the voltage sensor does not behave as an ideal capacitor. The leftover estimates the nonlinear properties of the charge movement in the voltage sensor. That is to say, the leftover estimates the charge movement of the voltage sensor that is ***not*** proportional to the size of the voltage step used in the measurement. The leftover is called gating current here and in experimental papers.

The gating current reported in experiments [16] can miss a component of the displacement current of the voltage sensor, if it uses the linear subtraction to estimate i_x. These procedures can remove more than the current through the lipid membrane capacitor i_{cap}.

Clearly, some of the current produced by movements of the arginines in the voltage sensor will be a linear displacement current, a linear component of gating current and it would not be present in the reported gating current determined by some linear subtraction procedures. In particular, if the arginine system is present at the 'control' potential contributing a current linear in potential, this problem would occur. Of course, if the arginine system is immobilized and inactivated at the control potential and so contributes no current flow under that condition, this problem would not occur.

Other systems may contribute to the linear displacement current as well, for example, i) all sorts of experimental and instrumentation artifacts and ii) displacement current in the conduction channel itself. The conduction channel of field effect transistors produces a large displacement current often characterized as a capacitance that involves diffusion and is described by drift diffusion equations quite similar to the PNP equations of the open conduction channel.

Most systems have substantial motions that are linear in voltage (even if the system is labeled 'nonlinear'). The linear term is present in most systems, just as it is present in most Taylor expansions of nonlinear functions.

The linear component that can be missed in experiments, and removed in these calculations, may have functional and structural significance. The voltage sensor works by sensing voltage, for example, by producing a motion of arginines. That motion—the response of the voltage sensor in this model—includes a linear component. The signal passed to the conduction channel, to control gating, is likely to include or depend on the linear component of sensor function. Confusion will result if a significant linear component exists and is ignored when a model is created that links the voltage sensor to the gating process of the conduction channel. Direct measurements of the movement of arginines (e.g., with optical methods) are likely to include the linear component and so should ***not*** agree with experimental measurements of gating current or with the currents reported here if the linear component exists and is significant in size.

If the P/4 procedure subtracts a charge movement in a control system in which the arginines do not move at all (because they are immobilized and inactivated, in that sense), then the resulting estimate of gating current will contain a component linear in voltage. Thus, the interpretation of the corrected record depends on the details of immobilization and inactivation, topics that are beyond the scope of this paper and our present work.

REFERENCES

[1] Horng, T.L., T.C. Lin, C. Liu, and B. Eisenberg. 2012. PNP equations with steric

effects: a model of ion flow through channels. *J. Phys. Chem. B.* 116(37):11422-11441.
[2] Lin, T.C., and B. Eisenberg. 2014. A new approach to the Lennard-Jones potential and a new model: PNP-steric equations. *Comm. Math. Sci.* 12(1):149-173.
[3] Eisenberg, B., Y.K. Hyon, and C. Liu. 2010. Energy variational analysis EnVarA of ions in water and channels: field theory for primitive models of complex ionic fluids. *J. Chem. Phys.* 133:104104.
[4] Bezanilla, F., E. Perozo, and E. Stefani. 1994. Gating of K^+ channels : II. The components of gating currents and a model of channel. *Biophy. J.* 66:1011-1021.
[5] Eisenberg, B. 2016a. Conservation of Current and Conservation of Charge. https://arxiv.org/abs/1609.09175.
[6] Eisenberg, B. 2016b. Maxwell Matters. https://arxiv.org/pdf/1607.06691.
[7] Eisenberg, B., X. Oriols, and D. Ferry. 2017. Dynamics of current, charge, and mass. *Mol. Based Math. Biol*. 5:78-115. https://arxiv.org/abs/1708.07400.
[8] Trefethen, L.N. 2000. Spectral Methods in MATLAB. SIAM, Philadelphia.
[9] Ascher, U.M., and L.R. Petzold. 1998. Computer methods for ordinary differential equations and differential-algebraic equations. SIAM, Philadelphia.
[10] Shampine, L.F., and M.W. Reichelt. 1997. The MATLAB ODE Suite. *SIAM J. Sci. Comput*. 18:1–22.
[11] Shampine, L.F., M.W. Reichelt, and J.A. Kierzenka. 1999. Solving Index-1 DAEs in MATLAB and Simulink. *SIAM Rev*. 41:538–552.
[12] Sigg, D., F. Bezanilla, and E. Stefani. 2003. Fast gating in the Shaker K+ channel and the energy landscape of activation. *Proc. Natl. Acad. Sci. USA.* 100:7611-7615.
[13] Stefani, E., and F. Bezanilla. 1997. Voltage dependence of the early events in voltage gating. *Biophys. J.* 72:131.
[14] Stefani, E., D. Sigg, and F. Bezanilla. 2000. Correlation between the early component of gating current and total gating current in Shaker K channels. *Biophys. J.* 78:7.
[15] Forster, I.C., and N.G. Greeff. 1992. The early phase of sodium channel gating current in the squid giant axon. Characteristics of a fast component of displacement charge movement. *Eur. Biophys. J.* 21(2): 99-116.
[16] Schneider, M.F., and W.K. Chandler. 1973. Voltage dependent charge movement in skeletal muscle: a possible step in excitation contraction coupling. *Nature.* 242:244-246.

[17] Armstrong, C.M., and F. Bezanilla. 1974. Charge movement associated with the opening and closing of the activation gates of the sodium channels. *J. Gen. Physiol.* 63:533-552.
[18] Bezanilla, F., and J. Vergara. 1980. Properties of Excitable membranes. *In* Membrane structure and Function. E.E. Bittar, editor. Vol. II, Ch. 2. J. Wiley & Sons, New York, 53-113.
[19] Bezanilla, F., and C.M. Armstrong. 1977. Inactivation of the sodium channel. I. Sodium current experiments. *J. Gen. Physiol.* 70(5):549-566.
[20] Fernández, J.M., F. Bezanilla, and R.E. Taylor. 1982. Distribution and kinetics of membrane dielectric polarization. II. Frequency domain studies of gating currents. *J. Gen. Physiol.* 79(1):41-67.